UCRL-JC-122333
PREPRINT
CONF-951182--8

Three-Dimensional Simulations of Nova Capsule Implosion Experiments

M. M. Marinak, R. E. Tipton, O L. Landen,
T. J. Murphy, S. W. Haan, C. J. Keane,
R. McEachern, and R. Wallace

This paper was prepared for submittal to the
37th Annual Meeting of the American Physical Society
Division of Plasma Physics
Louisville, KY
November 6-10, 1995

November 1, 1995

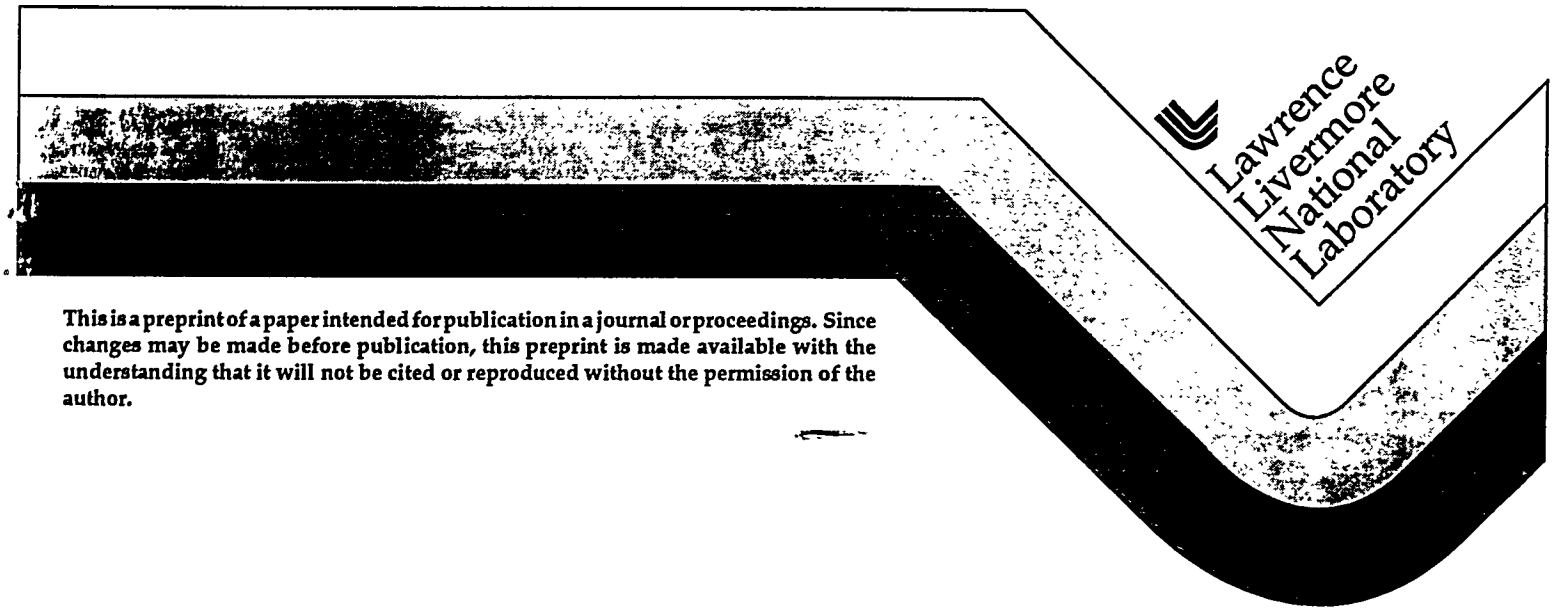

DISCLAIMER

Three-Dimensional Simulations of Nova Capsule Implosion Experiments

M. M. Marinak, R. E. Tipton, O. L. Landen,
T. J. Murphy, S. W. Haan, C. J. Keane, R. McEachern and R. Wallace
Lawrence Livermore National Laboratory,
Livermore, California 94551
(October 31, 1995)

Capsule implosion experiments carried out on the Nova laser are simulated with the three-dimensional HYDRA radiation hydrodynamics code [21]. Simulations of ordered near single mode perturbations indicate that structures which evolve into round spikes can penetrate farthest into the hot spot. Bubble-shaped perturbations can burn through the capsule shell fastest, however, causing even more damage. Simulations of a capsule with multimode perturbations shows spike amplitudes evolving in good agreement with a saturation model during the deceleration phase. The presence of sizable low mode asymmetry, caused either by drive asymmetry or perturbations in the capsule shell, can dramatically affect the manner in which spikes approach the center of the hot spot. Three-dimensional coupling between the low mode shell perturbations intrinsic to Nova capsules and the drive asymmetry brings the simulated yields into closer agreement with the experimental values.

52.35.Py, 47.40.-x, 52.65.+z, 52.70.La

I. INTRODUCTION

Hydrodynamic instabilities are of critical importance in inertial confinement fusion (ICF) since they place fundamental limits on the design parameters required for capsule ignition. The ablation surface of the capsule shell is subject to the Rayleigh-Taylor (RT) instability [1,2] as the shell accelerates inward. Short wavelengths (<30 μm) are stabilized on this surface by the effect of ablation and finite density gradients. Richtmyer-Meshkov [3,4] type growth also occurs due to perturbations on all interfaces. Perturbations grow and feed through to the fuel-pusher interface which is RT unstable during deceleration. If spikes on the fuel-pusher interface grow sufficiently large they will quench ignition.

Simulations of ablative RT growth on realistic 3-D surfaces are of interest for a number of reasons. For one the perturbations shape is a key factor in determining RT growth in the nonlinear regime. Experiments done with planar foils driven by x-rays show that symmetric three-dimensional (3-D) perturbations grow largest in the nonlinear regime, in agreement with simulations done with the HYDRA 3-D radiation hydrodynamics code [5]. A similar quantitative dependence of nonlinear saturation amplitude upon perturbation shape was obtained in simulations of foils driven directly by laser light [6,7]. Simulations of RT growth on classical interfaces in planar geometry [8,9], 2-D cylindrically symmetric geometry [9] and 3-D converging geometry [10,11] have also exhibited this shape dependence.

Surfaces of ICF capsules contain perturbations characterized by a variety of wavelengths and shapes. We have been using a model derived by Haan [12] to predict the magnitude of multimode RT growth at the fuel-pusher interface in a capsule implosion. A fundamental condition for applicability of the model is that nonlinear perturbation growth is dominated by saturated growth of long-wavelength modes present in the initial perturbation. This model is supported by 2-D simulations of capsules [13] as well as 3-D simulations of planar foils [7,14]. A three-dimensional simulation of a capsule implosion can examine whether the larger nonlinear growth which occurs in three dimensions causes strongly nonlinear behavior and consequent loss of memory of the initial perturbation [15,16] in convergent geometry. It also allows us to benchmark the model and check its treatment of complications introduced by time-varying wavelengths.

This paper presents the first 3-D simulations of capsule implosions ablatively driven by x-rays. These study high growth factor Nova capsule implosions [17] which have higher convergence than earlier experiments [18] and thus more sensitivity to asymmetry in the x-ray drive in a Nova hohlraum. Sizable low mode asymmetries are intrinsic to these Nova capsules. Since saturation amplitudes are proportional to wavelength these low modes can achieve large amplitudes. Individually these modes would be expected to cause gross asymmetry in the shell, resulting in little mix. But combined effects could be important. Simulations in three-dimensional allow us to explore the significance of such effects for capsule performance.

Section II of this article will discuss some details of the numerical simulations. Section III will examine how the shape of ordered near single mode perturbations effects how they feed through the capsule and grow. In section IV the evolution of multimode random perturbations will be examined. Finally section V considers the effect of radiation asymmetry, including the effects of coupling with surface perturbations.

II. NUMERICAL SIMULATIONS

Simulations presented here were performed with the HYDRA 3-D radiation hydrodynamics code [21]. HYDRA is based upon a structured mesh and has arbitrary Lagrangian Eulerian capability (ALE). An operator splitting procedure is used to treat each of the physical properties separately and combine the results. The Lagrange phase solves the compressible hydrodynamic equations, using a monotonic form of artificial viscosity [22], with predictor-corrector time stepping. A control volume technique is used to calculate surface areas and volumes of the hexahedral elements. It results in a consistent set of surfaces and consistent volumes on distorted meshes while conserving momentum. Van Leer advection [23] is employed in these simulations. The multigroup radiation diffusion routine incorporates a Von Neumann conjugate gradient matrix solver. For simulations of Nova capsules tabular XSN average-atom opacities are used [24], along with the Quotidian equation of state. Conductivities in the thermal conduction package are calculated according to the model of Lee and More [25]. These multi-material capsule simulations employ an Eulerian interface tracker, which is based upon the volume fraction method [26], generalized to run on arbitrary hexahedrons.

III. NEAR SINGLE MODE PERTURBATIONS

Fig. 1 shows a schematic of a Nova capsule which has a radius of 265 μm. To create these capsules a 220 μm inner radius polystyrene (CH) microballoon (wall thickness 3 $\pm$ 0.5 μm) is coated with a (3 $\pm$ 0.5 μm) layer of polyvinyl alcohol (PVA) which acts as a permeation barrier. An overcoating of CH ablator doped with 1.25 % (atomic) Ge gives a total wall thickness of 45 μm. The germanium dopant increases hydrodynamic instability growth and reduces x-ray preheat of the fuel. The capsule is enclosed in a 2400 μm long, 1600 μm diameter gold hohlraum. The convergence, defined here as the ratio of the initial outer ablator radius to the fuel radius

at bang time, is ~13 for these implosions. Further information about these implosion experiments can be found in references [19] and [20].

The measured radiation drive history is imposed on the capsule in the simulation (shown in Fig. 2 of reference [20]). It corresponds to the solid angle average of spectra from the wall and the laser spot. The shape of this drive spectrum is obtained from a LASNEX [27] hohlraum simulation with the M-band portion ($h\nu$ = 2-4 keV) renormalized to match the history of the experimental measurement. First we consider capsules with ordered near single mode perturbations. These are created by ablating pits (75 μm diameter) with an excimer laser [28] at the 92 locations corresponding to the vertices and face centers of the pattern on a soccer ball. Nearly all of the power in the surface perturbation spectrum is concentrated in spherical harmonic modes with l values near 18, which is believed to be the most dangerous range of modes for the capsule. If one hemisphere of this pattern is rotated azimuthally by 36 degrees, reflection symmetry is obtained about the equator, with a negligible effect upon spacing between pits or the perturbation mode spectrum. This geometry is treated exactly by simulating a domain which encompasses 1/20 of a sphere, extending from the pole to the equator and 36 degrees in azimuthal angle, with symmetry conditions at transverse boundaries. The grid used for most of these 1/20 sphere simulations measures 96x32x166 zones in the polar, azimuthal and radial directions respectively. Since the pattern possesses near hexagonal symmetry it can also be simulated over a small patch near the equator, in the absence of other sources of asymmetry, to obtain essentially the same quantitative results.

Simulations have been carried out for pit depths of 0.25, 0.5, 1.25 and 2.5 μm. Pits undergoing RT growth in the ablator maintain a constant solid angle as the shell implodes. In the deceleration phase fuel bubbles rise at the initial locations of the pits, as shown in Fig. 2, for a case with 0.5 μm initial pit depth. A Kelvin-Helmholtz instability causes roll up at the classical fuel-pusher interface. This roll up is asymmetric, concentrated at the bubble tips as a result of the bubble-like shape of the initial perturbations. Interconnecting spike sheets of pusher material fall inward between the bubbles. The evolution of the 2.5 μm case is qualitatively different from the others because the bubble penetrates the shell. Fig. 3 compares the minimum fuel-pusher radius vs. time for an unperturbed capsule and a capsule with pits 2.5 μm deep. The shock breaks out of the shell behind the pits significantly earlier than for the remainder of the shell, giving a noticeable inward displacement. After 1.8 ns the bubble tips accelerate inward as the shell grows thin ahead of them, leading to a highly elongated shape. By 1.9 ns the bubble, which consists of low density ablator material, has grown through the higher density layers of PVA and polystyrene mandrel and has come into contact with the fuel. As a result a jet of mandrel material forms in a ring in front of the bubble tip. This jet encounters the rebounding shock sooner than the rest of the shell, enhancing spike growth. The fall line, which is often cited as a pessimistic limit of spike growth, is obtained by extrapolating using the maximum inward slope of the unperturbed interface trajectory. The spike is seen to reach the center of the capsule before the fall line.

When we reverse the sign of the initial perturbation the fuel-pusher interface develops round spikes surrounded by rising bubble ridges during deceleration. The Kelvin-Helmholtz roll up at the fuel-pusher interface is again asymmetric, but this time it is concentrated at the tip of the round spikes. For both topologies simulated here the close packing of the spikes results in a large pressure gradient forming across the spike tips as they converge toward the capsule center, slowing their fall. These two topologies, round spikes surrounded by bubble ridges and spike ridges surrounding round bubbles, were also seen in hydrodynamic simulations of the classical RT instability in a decelerating capsule shell [11].

We have compared neutron yields for the two perturbation shapes versus initial perturbation amplitude. The perturbation consisting of individual bumps is found to cause more yield degradation than the pit perturbations for each of the three smallest amplitudes. But for the 2.5 μm amplitude the pit perturbation results in the lowest yield, since it burns through the shell, thereby enhancing spike growth. For all cases there is a strong connection between neutron yield and the spike amplitude at bang time.

Conceptually we can consider the perturbation amplitude attained on the fuel-pusher interface to be the product of three factors: (1) the amplitude of the perturbation at the ablation front during the implosion phase, (2) a feed through factor relating the perturbation amplitudes at the inner and outer shell surfaces at the onset of deceleration, and (3) growth of the perturbation on the inner shell during deceleration. We compare measures of each of these quantities for the two 3-D shapes described above and for a 2-D axisymmetric $cos(18\,\theta)$ perturbation. The 2-D simulation is carried out over 1/2 wavelength adjacent to the equator. Although this perturbation is not an eigenmode, it avoids introducing a 3-D bubble or spike at the pole. The ablation front amplitude, defined in terms of displacement of the density isocontour $\rho_{max}/2$, is similar for all three shapes at the onset of deceleration for a given initial amplitude. It is linearly proportional to initial perturbation amplitude up to a/λ at deceleration equal to 0.25, above which the effect of saturation becomes apparent. The extent to which the perturbation feeds through the shell is virtually identical for all three mode shapes and essentially independent of perturbation amplitude well into the nonlinear regime, as long as the bubble does not penetrate the shell.

Nonlinear growth rates in the fuel-pusher interface during deceleration show a clear dependence upon perturbation shape. Except for the cases with large amplitude perturbations, where the shell burns through or spikes approach close to the center early, the elongated spike

sheets which develop on capsules with 3-D pit perturbations grow at the same rate as the 2-D axisymmetric spike. The round 3-D spikes which form from the bump perturbations grow faster. Likewise the elongated bubble ridges which develop on capsules with 3-D bump perturbations rise at the same rate as the 2-D bubbles. The round bubbles resulting from the 3-D pit perturbations rises much faster. They accelerate as the shell material thins above them, exhibiting rise velocities much greater than the asymptotic Layzer velocity, which was derived for a semi-infinite medium [29]. The differences in rise velocities can be understood in terms of the perturbation shapes. For round 3-D bubbles material can flow into the spikes from all sides, resulting in a higher bubble rise velocity.

IV. MULTIMODE CAPSULES

Experiments on Nova have also examined the behavior of capsules with various amplitudes of imposed multimode surface perturbations [17]. Pits are ablated at 200 randomly selected locations which are the same for each capsule. The perturbation initialized over the 1/20 sphere domain is based on the pattern from a portion of the actual surface. The mode spectrum is projected onto spherical harmonics compatible with the symmetry boundary conditions, namely m values which are multiples of 5 and l+m even. This representation maintains information on the perturbation shape. The pits on the initial surface often overlap, as is apparent in Fig. 4. A single pit feature near the equator in Fig. 4 has ~3.5 times the depth on an individual pit. The symmetry of the domain results in 5 such pits over the entire sphere, which corresponds to the number of locations where ~4 pits overlap on the actual surface. In addition the smoothed spectrum of the simulated surface closely resembles the power spectrum from the full surface.

We consider a capsule with the multimode random perturbation scaled to 0.15 μm rms amplitude. The perturbations which grow on the ablation surface and then on the fuel-pusher interface early in the deceleration phase strongly resemble the topology of the imposed perturbation. Fuel bubbles rising at the locations of the initial pits have shapes and amplitudes which correspond to the pit perturbations initially imposed. At 2.00 ns, when the bubble heights are similar to their widths, a series of interconnecting spike sheets are falling between them. By 2.05 ns a round spike which has developed on axis has penetrated noticeably further than the spike sheets. As these spike structures converge toward the center they develop pointed shapes. The Kelvin-Helmholtz roll up at the bubble tips, shown in Fig. 5, resembles the development of individual bubbles resulting from the "soccer ball" pattern.

The evolution of the perturbation spectrum in the shell can be examined by decomposition of the mass mode amplitude $M(\theta,\phi) = \int \rho(\theta,\phi) r^2 dr$ into spherical harmonics. The power spectrum obtained from the spherical harmonic coefficients shows that modes which arise from mode coupling do not dominate the evolution for times of interest. The majority of power remains in modes with l values characteristic of the initial perturbation spectrum. This is a fundamental condition for applicability of the Haan saturation model [12], which we have been using to calculate amplitudes of multimode perturbations in capsules. These amplitudes are obtained from a quadrature sum over the set of individual mode amplitudes determined using linear growth factor calculations. Individual modes grow linearly until a saturation amplitude $\nu R/l^2$ is obtained, upon which the growth switches to secular. A value of $\nu = 2$ is used for the saturation parameter based upon results from recent simulations and experiments [7,14,30].

To compare the 3-D calculation with the model we will define the spike penetration according to the radius where 10% of the surface is occupied by spikes of pusher material. The distance between this position and the position obtained for an unperturbed interface is taken as the spike amplitude. For the 0.15 μm rms perturbations we find good agreement between the time histories of spike growth from the 3-D calculation and the saturation model during the deceleration phase. At the time of peak neutron production for an unperturbed capsule the 3-D multimode simulation gives a spike amplitude of 7.5 μm vs. 6.7 μm for the saturation model. The result changes little if we use a spike amplitude defined using the surface covered by 1% spike material. The largest bubbles in the 3-D simulation rise with velocities much greater than the Layzer asymptotic velocity, and they accelerate as the shell thins ahead of them. Consequently the maximum bubble amplitudes are much larger than predicted by the saturation model, which was designed to give bubble growth rates like Layzer's. For example at the time referenced above the 3-D simulation gives a bubble amplitude of 16.5 μm vs. 5.1 μm for the saturation model. We note that the model prescription for saturated growth results in an rms perturbation amplitude which decreases with time for the last 100 ps prior to the onset of deceleration. This is due to the decrease in modal saturation amplitude $\nu R(t)/l^2$ caused by shell convergence. In the 3-D simulation bubble growth *rates* drop as the wavelength decreases due to convergence of the shell. But perturbation amplitudes do not decrease during this period. In the 1-D mix model, which we have been using to model capsule performance, regions within the mixing lengths, determined from the saturation model, on each side of the fuel-pusher interface are subject to thermal and atomic mixing. Details of the 1-D mix model have been described elsewhere [20]. The neutron yield calculated with the model for a capsule with the 0.15 μm rms perturbation is 8.2×10^8. This compares with a yield of 1.26×10^9 from the HYDRA simulation of the 0.15 μm capsule and 2.5×10^9 for an unperturbed capsule.

V. EFFECTS OF DRIVE ASYMMETRY

Although the 1-D mix model compares reasonably well with the 3-D simulation of the Nova capsule with an imposed surface perturbation, it does not take into account the effects of other sources of asymmetry, such as the x-ray drive. Five beams enter each end of the Nova hohlraum forming rings located on the wall so as to minimize the time-averaged asymmetry in the x-ray flux. Even with perfect pointing and power balance between beams low mode asymmetries arise due to motion of the laser spots [31]. Principal among these is the time-varying pole-waist radiation flux variation, which can be characterized in terms of a Y_{20} spherical harmonic (or P_2 Legendre polynomial). The azimuthal variation associated with the laser spots has a fundamental period corresponding to m=5, which can be simulated over the 1/20 sphere domain described earlier. Time varying m=0 components of drive asymmetry imposed on the capsule in the HYDRA simulation are obtained from a LASNEX hohlraum simulation. The azimuthally varying components of the drive asymmetry are obtained from an analytic estimate which uses a calculated time-varying albedo. Contributions to asymmetry due to pointing errors and beam power imbalance are not modelled.

Fig. 6 shows the fuel-pusher interface 30 psec after bang time. Coefficients of the m=5 components imposed have smaller average magnitudes than for the P_2 and P_4. But the higher Rayleigh-Taylor growth rates of the m=5 terms leads to greater amplification on the capsule. Bubbles are rising half way between the hohlraum equator and the pole, nearest the locations of the laser spots. Spikes are rapidly approaching the center of the hot spot near the equator. These reach the center of the hot spot after the bang time calculated for an unperturbed, spherical implosion and thus have only a modest effect on the yield. The calculated yield, 1.44×10^9, is equal to 59% for a perfectly spherical implosion, and 92% of the clean yield when only m=0 terms are included.

Even for the smallest imposed perturbations on these Nova capsules nonlinear coupling between drive asymmetry and surface perturbations is important. When drive asymmetry is added into the simulation of the capsule with the 0.5 μm "soccer ball" perturbation nonlinear coupling results in the formation of large spikes at the equator. In the early stages of deceleration, between 1.9 and 2.0 ns, the amplitude of these spikes is essentially equal to the sum of spike amplitudes obtained from separate simulations having drive asymmetry or 0.5 μm soccer ball perturbations alone. The presence of the low mode drive asymmetry causes the spikes at the equator to approach the capsule center rather sooner than the others. There is ample room for fuel in the asymmetric core to flow around these spikes. This factor, combined with the round shape of these spikes, allows them to continue nearly in free fall, arriving at the capsule center before the fall line. This scenario is not specific to the soccer ball pattern. When drive asymmetry is included the capsule having the 0.15 μm rms multimode surface perturbation also develops a spike of nearly the same size, nearly in free fall, at a location slightly off of the equator.

Fig. 7 shows experimental yields for capsules having "soccer ball" and multimode perturbations of various amplitudes, shown as open and solid circles respectively. The intrinsic surface roughness of smooth capsules is reported according to the sum from the measured spectrum for modes having $l > 10$. Based on this convention the intrinsic roughness for smooth capsules is listed as < 0.05 μm. Predicted yields for the multimode capsules obtained from the 1-D mix model are shown as crosses. There is good agreement between the 1-D model and experimental yields for rough capsules. But the improvement in the experimental yield for smoother capsules is substantially less than the 1-D model predicts.

Calculated neutron yields from the 3-D simulations of capsules having imposed multimode or soccer ball patterns, including drive asymmetry effects, are also shown in Fig. 7 as solid and open squares respectively. For the 0.15 μm rms amplitude the simulated yields are similar for both types of imposed perturbations, just as in the experimental data. We note that these two simulations do not include surface roughness intrinsic to these capsules.

Roughness of the capsule surface is quantified from a series of circumferential depth profiles recorded by atomic force microscopy and from interferometry measurements. These newly-developed techniques provide reliable measurements of the low mode components ($l < 10$) of intrinsic capsule asymmetry which were unavailable in past experimental campaigns. The measurements show that the smooth capsules have large low-l mode components. Interferometry indicates a typical P_1 perturbation in shell concentricity is 4 μm peak to valley. Very low mode surface perturbations undergo little RT growth; their growth results mostly from capsule convergence. Individually they cause gross asymmetries in the capsule shape, but result in little mix. We consider how the combined effects of very low mode surface perturbations and drive asymmetry can affect the performance of a Nova capsule. Since the coupling depends on how the very low mode perturbations are oriented relative to the hohlraum axis the effect of coupling would have a stochastic signature in the experimental yields. To examine one limit a simulation included the capsule intrinsic surface roughness resulting from modes with $l > 10$ only and included drive asymmetry. It produced a yield of 1.37×10^9, shown as the square symbol at 0.02 μm rms in Fig. 7. In a second simulation very low mode asymmetries were also included giving a peak-to-valley amplitude typical of measured values. These modes were oriented so as to enhance the effect of coupling with drive asymmetry. In the latter case the spikes reached the center of the capsule 50 ps sooner than in the former case, causing the yield to be reduced to 6.0×10^8, as represented by the triangle in Fig. 7. This preliminary result suggests that coupling between low mode capsule shell perturbations

and drive asymmetry can explain much of the variability in the yields of the smooth germinated capsules and bring simulated yields closer to the experimental values. The calculated yields for the capsules with 0.15 μm imposed surface perturbations are also expected to move closer to the experimental values when the intrinsic low mode asymmetries are included.

VI. CONCLUSIONS

We have presented results from the first 3-D simulations of capsule implosions ablatively driven by x-rays. Simulations of the growth of ordered near single mode perturbations indicate that structures which evolve into round spikes can penetrate farthest into the hot spot. A bubble-shaped perturbation is capable of burning through the capsule shell fastest. In cases when a bubble in the ablator burns through the shell even larger spike growth occurs, resulting in a greater reduction in neutron yield. For a Nova capsule a large reduction in yield occurs only when spikes of pusher material crash into the center of the hot spot during the period of peak neutron production.

Simulations have also examined the growth of multimode surface perturbations created on Nova capsules by ablating pits at random locations. For a capsule with a 0.15 μm rms perturbation growth remains dominated by modes initially present on the capsule rather than modes driven by mode coupling. Spike amplitudes calculated for the fuel-pusher interface according to the Haan saturation model [12] are in good agreement with values from the 3-D simulation during the deceleration phase. The largest bubbles rise much faster then predicted by the model, however, due to the effect of of finite shell thickness.

The presence of sizable low mode asymmetry caused either by drive asymmetry or perturbations in the capsule shell can dramatically affect the manner in which spikes approach the center of the hot spot. The low mode asymmetry combined with the growth of individual shorter wavelength spikes causes a few spikes to approach the capsule center rather sooner than the rest. These are not subject to the same retarding pressure gradient which develops when a densely packed array of spikes approach the center. These few spikes will tend to grow more round and continue toward the center of the hot spot, nearly in free fall. Simulations show that very low mode asymmetry intrinsic to Nova capsules couples with x-ray drive asymmetry to generate spikes which reached the center of the hot spot in time to reduce capsule yield. Preliminary results suggest that the dependence of this coupling on the alignment of very low mode perturbations relative to the laser spot pattern can explain much of the variability in experimental yields of smooth germanium-doped capsules. When the effects of drive asymmetry and low mode intrinsic capsule asymmetry are included the 3-D simulations produce yields which are closer to the experimental yields across a range of imposed surface perturbation amplitudes.

ACKNOWLEDGEMENTS

We wish to thank Steve Hatchett for analysis of the azimuthal drive asymmetry and B. Remington and S. Weber for reviewing this manuscript. We acknowledge the support of the technical staff at Nova. This work was performed under the auspices of the U.S. DOE by the Lawrence Livermore National Laboratory under Contract No. W-7405-ENG-48.

---

[1] J. D. Lindl and W. C. Mead, Phys. Rev. Lett. **34**, 1273 (1975).

[2] S. E. Bodner, Phys. Rev. Lett. **33**, 761 (1974).

[3] R.D. Richtmyer, Commun. Pure Appl.. Math. **13**, 297 (1960); E. E. Meshkov, Izv. Akad. Nauk SSSR, Mekh. Ahidk. Gaza **5**, 151 (1969).

[4] G. Dimonte and B. Remington, Phys. Rev. Lett. **70**, 1806 (1993).

[5] M. M. Marinak, B. A. Remington, S. V. Weber, R. E. Tipton, S. W. Haan, K. S. Budil, O. L. Landen, J. D. Kilkenny and R. Wallace, Phys. Rev. Lett., accepted for publication.

[6] J. P. Dahlburg, J. H. Gardner, G. D. Doolen, and S. W. Haan, Phys. Fluids B **5**, 571 (1993).

[7] J. P. Dahlburg, D. E. Fyfe, J. H. Gardner, S. W. Haan, S. E. Bodner, G. D. Doolen, Phys. Plasmas **2**, 2453 (1995).

[8] G. Tryggvason and S. O. Unverdi, Phys. Fluids A **2**, 656 (1990).

[9] T. Yabe, H. Hoshino, and T. Tsuchiya, Phys. Rev. A **44**, 2756 (1991).

[10] H. Sakagami and K. Nishihara, Phys. Rev. Lett. **65**, 432 (1990).

[11] R. P. J. Town and A. R. Bell, Phys. Rev. Lett. **67**, 1863 (1991).

[12] S. W. Haan, Phys. Rev. A, **39**, 5812 (1989).

[13] S. W. Haan, S. M. Pollaine, J. D. Lindl, L. J. Suter, R. L. Berger, L. V. Powers, W. E. Alley, P. A. Amendt, J. A. Futterman, W. K. Levedahl, M. D. Rosen, D. P. Rowley, R. A. Sacks, A. I. Shestakov, G. L. Strobel, M. Tabak, S. V. Weber, G. B. Zimmerman, W. J. Krauser, D. C. Wilson, S. V. Coggenshall, D. B. Harris, N. M. Hoffman, B. H. Wilde, Phys. Plasmas **2** 2480 (1995).

[14] M. M. Marinak, R. E. Tipton, B. A. Remington,and S. V. Weber, Bull. Am. Phys. Soc., **39**, 1684 (1994).

[15] D. Shvarts, U. Alon, D. Ofer, R. L. McCrory and C. P. Verdon, Phys. Plasmas **2** 2465 (1995).

[16] D. L. Youngs, Proceedings of the *4th International Workshop on the Physics of Compressible Turbulent Mixing*, edited by P. F. Linden, D. L. Youngs, and S. B. Dalziel (Cambridge Univ. Press, Cambridge, 1993), p. 167.

[17] O. L. Landen, C. J. Keane, B. A. Hammel, M. D. Cable, J. Colvin, R. Cook, T. R. dittrich, S. W. Haan, S. P. Hatchett, R. G. Hay, J. D. Kilkenny, R. A. Lerche, W. K. Levedahl, R. McEachern, T. J. Murphy, M. B. Nelson, L. Suter, and R. J. Wallace, J. Quant. Spectrosc. Radiat. Transfer **54** 245 (1995).
[18] T. R. Dittrich, B. A. Hamel, C. J. Keane, R. McEachern, R. E. Turner, S. W. Haan, and L. J. Suter, Phys. Rev. Lett. **73**, 2324 (1994).
[19] O. L. Landen, et al., these proceedings.
[20] C. J. Keane, G. W. Pollak, R. C. Cook, T. R. Dittrich, B. A. Hammel, O. L. Landen, S. H. Langer, W. K. Levedahl, D. H. Munro, H. A. Scott, and G. B. Zimmerman, J. Quant. Spectrosc. Radiat. Transfer **54**, 207 (1995).
[21] M. M. Marinak, R. E. Tipton, B. A. Remington, S. W. Haan, S. V. Weber, ICF Quarterly Report **5**, (1995) UCRL-LR-105821-95-3.
[22] D. J. Benson, Comp. Methods in Applied Mechanics and Engineering, **93** (1991) 39-95.
[23] B. Van Leer, J. Comp. Phys., **23**, 276 (1977).
[24] See National Technical Information Service Document No. UCRL-52276 [W. A. Lokke and W. H. Grasberger, in Lawrence Livermore National Laboratory Report No. UCRL-52276 (1977)]. Copies may be ordered from National Technical Information Service, Springfield, VA 22161. G. B. Zimmerman and R. M. More, J. Quant. Spectrosc. Radiat. Transfer **23**, 517 (1980); R. M. More, *ibid.* **27**, 345 (1982).
[25] Y. T. Lee and R. M. More, Phys. Fluids **27**, 1273 (1984).
[26] D. L. Youngs, in *Numerical Methods for Fluid Dynamics*, edited by K. W. Morton and M. J. Baines (Academic, New York, 1982).
[27] G. B. Zimmerman and W. L. Kruer, *Commun. Plasma Phys.*, **11**, 51 (1975).
[28] R. J. Wallace, R. L. McEachern, and W. W. Wilcox, ICF Quarterly Report **4**, 79 (1994), UCRL-LR-105821-94-3.
[29] D. Layzer, Astrophys. J. **122**, 1 (1955).
[30] M. J. Dunning and S. W. Haan, Phys. Plasmas **2**, 1669 (1995).
[31] L. J. Suter, A. A. Hauer, L. V. Powers, D. B. Ress, N. Delameter, W. W. Hsing, O. L. Landen, A. R. Thiessen, And R. E. Turner, Phys. Rev. Lett., **73**, 2328 (1994).

FIG. 1. Schematic of a capsule used in the implosion experiments simulated.

FIG. 2. Iso-density contours of 17 g/cm^3 shown near bang time for a portion of a capsule with 0.5 μm deep pits imposed in the "soccer ball" pattern. The lighter outer surface is in the ablation region, while the darker inner surface corresponds to the fuel-pusher interface. The white curves outline the angular extent of the 1/20 sphere region simulated.

FIG. 3. Minimum spike radius vs. time for an unperturbed capsule (solid), and a capsule having pits 2.5 μm deep imposed in the "soccer ball" pattern (dashed). The dash-dot trace indicates the fall line.

FIG. 4. Contours showing locations of the initial perturbations for the multimode pattern simulated.

FIG. 5. A hemispherical portion of the fuel-pusher interface seen from the outside at 2.05 ns for a capsule having a 0.15 μm multimode perturbation.

FIG. 6. Fuel-pusher interface for a spherical capsule subjected to x-ray drive asymmetry shown over a hemisphere 30 psec after bang time.

FIG. 7. Solid and open circles show experimental yields of Nova capsules having multimode and "soccer ball" perturbations of various amplitudes. The crosses indicate yields calculated with the 1-D mix model. The solid and open squares are from 3-D HYDRA simulations of capsules with multimode and "soccer ball" perturbations. The square at 0.02 μm is for a capsule simulated with drive asymmetry and the intrinsic surface perturbations due to modes with $l > 10$ only. The triangle represents a simulation which also includes intrinsic low mode asymmetries oriented so as to enhance the effect of coupling with drive asymmetry. For the 0.15 μm amplitudes only the imposed surface perturbations and drive asymmetry are included.

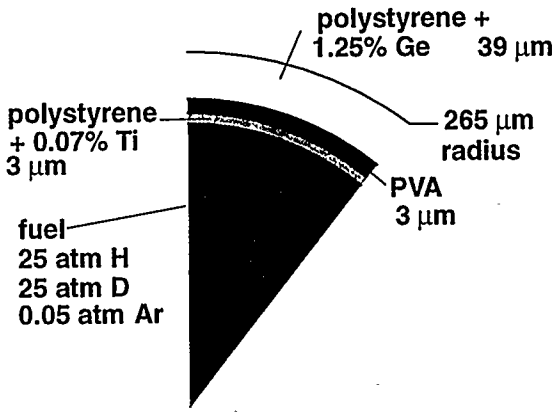
polystyrene +
1.25% Ge
39 μm
265 μm
radius
polystyrene
+ 0.07% Ti
3 μm
PVA
3 μm
fuel
25 atm H
25 atm D
0.05 atm Ar

Fig. 1

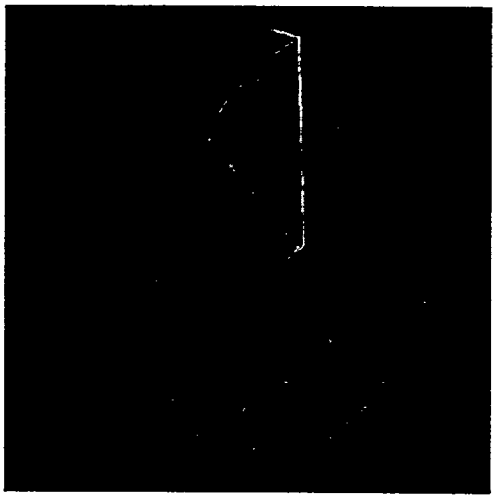

Fig. 2

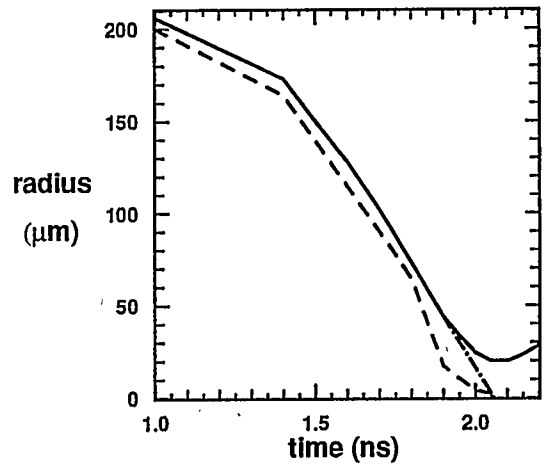

Fig. 3

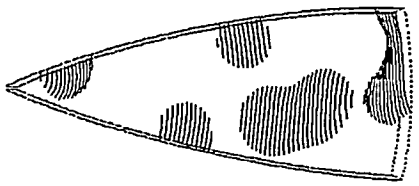

Fig. 4

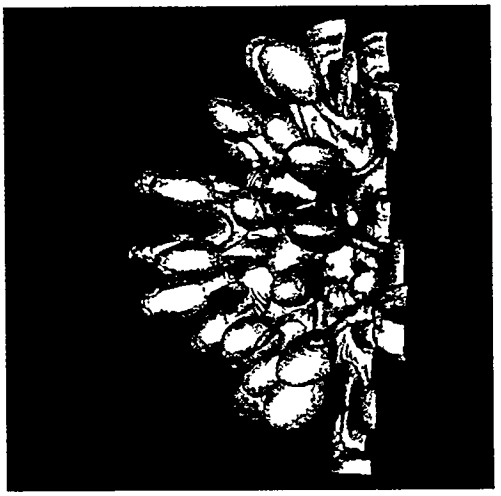

Fig. 5

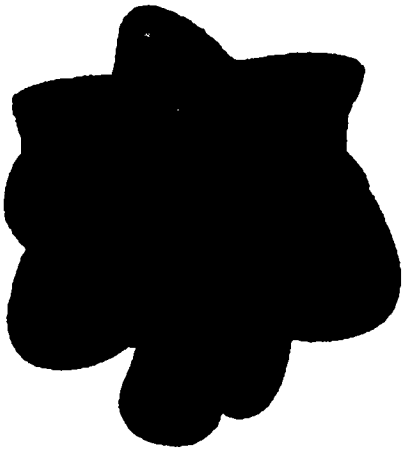

Fig. 6

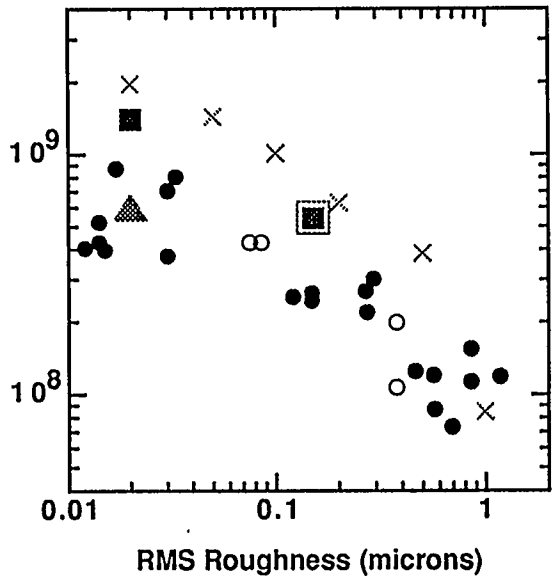

Fig. 7

Technical Information Department • Lawrence Livermore National Laboratory
University of California • Livermore, California 94551